ELSEVIER

Int. J. Therm. Sci. 41 (2002) 412–421

International Journal of Thermal Sciences

www.elsevier.com/locate/ijts

Radiative field and radiometric temperature measurements in semi-transparent films

Gennaro Cuccurullo *, Pier Giorgio Berardi

Dipartimento di Ingegneria Meccanica, Via Ponte Don Melillo, Fisciano (SA), Italy

Received 13 February 2001; accepted 17 July 2001

Abstract

The control of the temperature in many industrial processes takes place advantageously by means of infrared radiometers. The basic assumption for performing automatic temperature readout is the target grey body behaviour. This foundation fails in molten polymers processing operations, where materials and thickness are such that the semitransparent behaviour is enhanced, thus new ways are to be sought to carry out temperature detection.

This study aims to characterise infrared temperature measurements accounting for that portion of the radiation coming from the bulk, thus related to the inner temperature distribution. Having in mind operations involving molten polymers in free air, such as polymer extrusion, the polymer is sketched as a slab with known temperature distribution across the thickness and confined by a surrounding at known temperature. Features related to temperature readout performed with shortwave and longwave radiometers are evidenced.

Keywords: Infrared; Polymers; Extrusion; Thermography; Plastic; Radiation

1. Introduction

Recent advancements in infrared technology, such as the development of focal plane array systems, have provided better image resolution, interface friendly systems, while reducing system size and weight. At the same time, interest in using infrared cameras as predictive maintenance and process monitoring for plastic industry is continuously increasing: “hot spots” can be easily identified and repairs can be set-up, reducing equipment failure and avoiding costly production downtime. Furthermore, the ability of recording both thermal and visual images of targets can help to highlight problems during scheduled shutdowns.

Taking into account their short response time and their ability to perform non-contact temperature measurement, the control of the temperature by means of infrared radiometers seems to be particularly appropriate in operations involving molten polymers in free air, such as polymer extrusion. Extrusion is a method widely used in industry to process plastics: plastic is first heated above its glass transition temperature, so that it will flow, then is forced under high pressure through a slit die, is slightly stretched in the machine direction in air and last experiences a path in free air, in the region between die exit to chill roll, e.g., cast or buble film production. The route in air of the material from the die to the chill roll is essential in determining the final film properties, in fact strong variations in width, thickness and temperature take place in a short time, while the material becomes solid. Thus, the knowledge of temperature development along the path in free air represents a key parameter in order to control both the working process and the quality of the final product [1–5].

Monitoring with IR sensors for process control of these materials is documented in the literature [6–14]. As an example of qualitative process monitoring, unprocessed raw images are reported in next pictures concerning film casting, Fig. 1(a), and bubble extrusions, Fig. 1(b), on thermoplastic polymers, namely polyethylenetherephtalate (PET) and polypropylene (PP). The images are taken at different conditions of mass rate (U_0), drawing (U_L/U_0), cooling and take-up (L) distance. Different material behaviour are quite evident.

Wishing quantitative measurements, the semitransparent polymers behaviour in the bands usually sensed by available radiometers has to be taken into account. Polymers exhibit

* Correspondence and reprints.
E-mail address: gcuccurullo@unisa.it (G. Cuccurullo).

1290-0729/02/$ – see front matter
PII: S1290-0729(02)01333-9

Nomenclature

$+$	forward component	$e_{\Delta\nu,\omega}$	*radiometer-slab* emittance
$-$	backward component	$a_{\Delta\nu,\omega}$	*radiometer-slab* absorptance
T	temperature ..... K	$E_{\Delta\nu,\omega}$	basic radiometer-slab function
$I_{\nu\omega}$	directional spectral intensity ..... $W\cdot m^{-2}\cdot sr^{-1}$	*Greek symbols*	
x	spatial coordinate along the slab ..... m	ν	frequency ..... Hz
k_ν	spectral absorption coefficient ..... m^{-1}	ξ	spectral optical path
n_ν	spectral refractive index	ξ_L	optical thickness
$I_{b\nu}$	black body spectral intensity ..... $W\cdot m^{-2}\cdot sr^{-1}$	*Subscripts/Superscripts*	
L	slab thickness ..... m	0	interface at $x = 0$
$\tau_{\nu\omega}$	interface spectral directional transmittivity	L	interface at $x = L$
$\rho_{\nu\omega}$	interface spectral directional reflectivity	b	black body
$J_{\nu\omega}$	auxiliary bulk function ..... $W\cdot m^{-2}\cdot sr^{-1}$	ext	external
$T_{\nu\omega}$	spectral directional beam transmittance	$\perp$	normal surface direction
$t_{\nu\omega}$	spectral directional slab transmittance	ω	direction
$r_{\nu\omega}$	spectral directional slab reflectance	λ	wavelength ..... m
$a_{\nu\omega}$	spectral directional slab absorptance		
$e_{\nu\omega}$	spectral directional slab emittance		

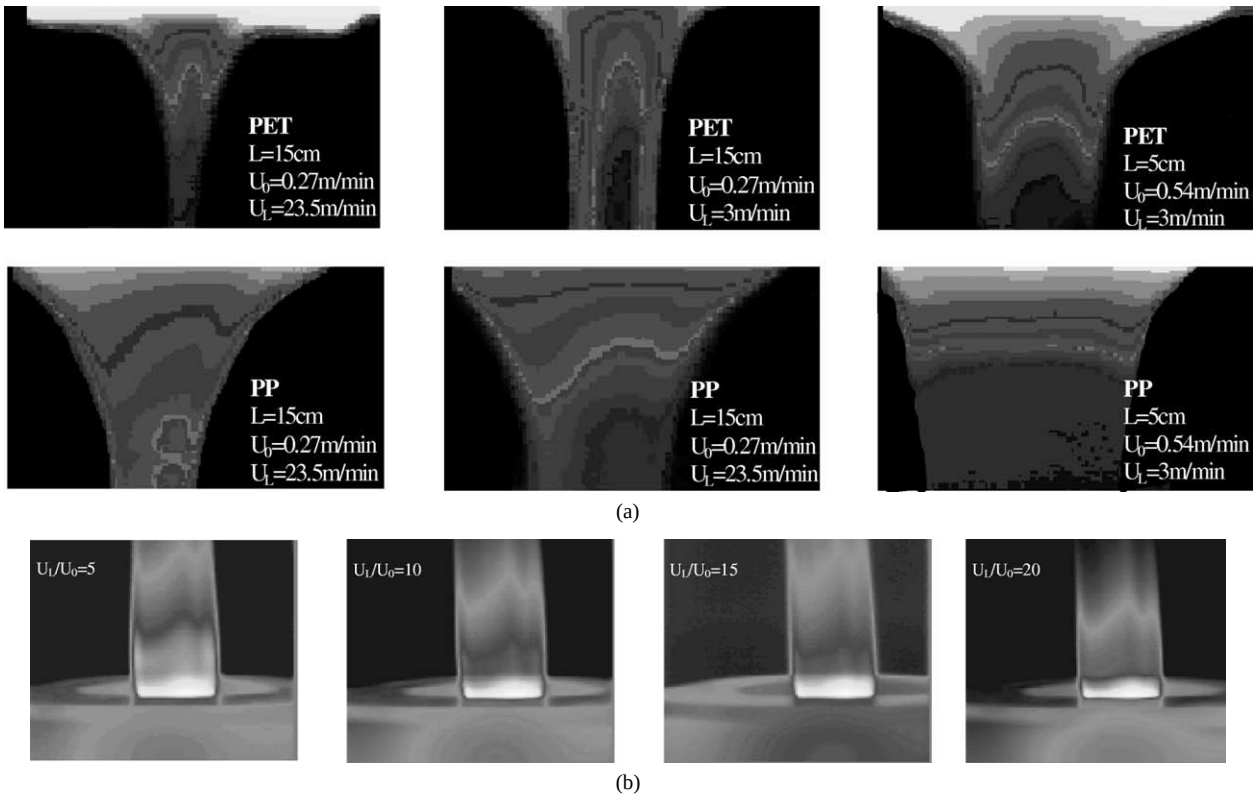

Fig. 1. (a) Pet and pp film casting extrusions; (b) Pet bubble extrusions.

a peek in the absorption band centred at 3.4 μm for carbon-hydrogen bonding, such as the polystyrene, and at 7.95 μm for the carbon-oxygen bonding, such as polyester [15]. For such materials and for typical film thickness, the temperature readout cannot be performed by automatic emissivity correction mode, based on the assumption that the target behaves as a grey body, and new ways are to be sought to carry out temperature detection. Temperature readout, unlike of what happens for opaque materials where the radiation is a superficial phenomenon, has to take into account that a portion of the radiation comes from the bulk, thus it is related to the inner temperature distribution.

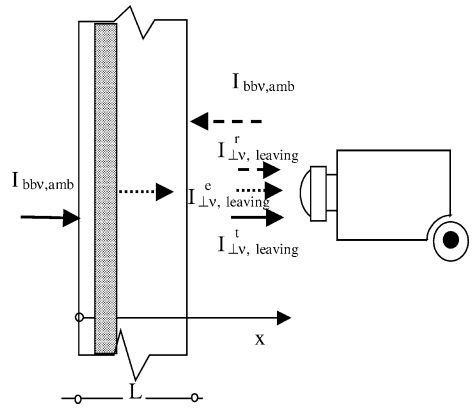

Fig. 2. Sketch of the problem.

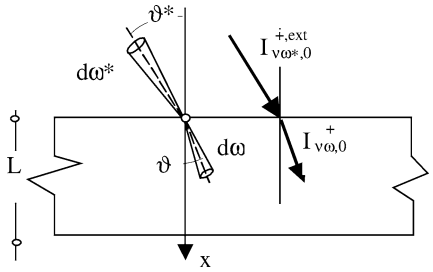

Fig. 3. Interface transmission.

In order to perform significant temperature readout, the present work deals with a simple model set-up for the radiative field in a plane plastic film; the model allows to evidence the key parameters influencing the temperature readout for different material and geometrical configurations, depending on the instrument in use.

2. Radiative field

A slab with a known temperature distribution, $T = T(x)$, is considered; the slab is embedded in air and confined by a surrounding such as the intensities incident on both faces are known. A radiometer looks the slab at a fixed angle to the surface. The problem is sketched in Fig. 4 for a right angle of view.

2.1. Radiative field inside the slab

The radiation field inside the slab can be obtained by solving the local radiant energy balance equation:

$$\mu\,\mathrm{d}I_{\nu\omega}(x)/\mathrm{d}x = k_\nu\left(n_\nu^2 I_{\mathrm{b}\nu} - I_{\nu\omega}\right) \tag{1}$$

where: $I_{\nu\omega} = I_{\nu\omega}(\nu, \vartheta, \varphi)$ is the directional spectral intensity in the direction $\omega(-\pi/2 \leqslant \vartheta \leqslant \pi/2, 0 \leqslant \varphi \leqslant 2\pi)$; $\mu = \cos(\vartheta)$; $I_{\mathrm{b}\nu} = I_{\mathrm{b}\nu}(\nu, T)$ is the Plank's function; k_ν and n_ν are the spectral absorption coefficient and the refractive index of the media.

The radiative behaviour of the slab material is described by two intensive parameters: the spectral absorption coefficient and the refractive index, both weakly dependent on temperature. Here they will be assumed temperature independent.

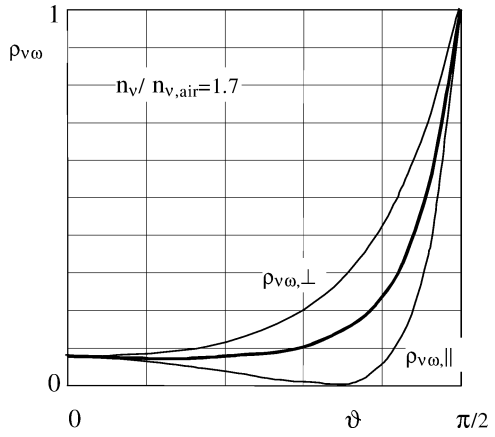

Fig. 4. External reflection.

The formal solution [16] to the radiative equation can be conveniently obtained with respect to the forward and backward intensity components, $I_{\nu\omega}^+$ and $I_{\nu\omega}^-$:

$$I_{\nu\omega}^+(\xi) = I_{\nu\omega,0}^+ \exp(-\xi/\mu) + \int_0^\xi n_\nu^2 I_{\mathrm{b}\nu}\left[T\left(\xi^*\right)\right]\exp\left[-\left(\xi-\xi^*\right)/\mu\right]\mathrm{d}\left(\xi^*/\mu\right) \tag{2}$$

$$I_{\nu\omega}^-(\xi) = I_{\nu\omega,L}^- \exp\left[-(\xi_L-\xi)/\mu\right] + \int_\xi^{\xi L} n_\nu^2 I_{\mathrm{b}\nu}\left[T\left(\xi^*\right)\right]\exp\left[-\left(\xi^*-\xi\right)/\mu\right]\mathrm{d}\left(\xi^*/\mu\right) \tag{3}$$

where: $I_{\nu\omega,0}^+ = I_{\nu\omega}^+(\xi = 0, \vartheta, \varphi)$ and $I_{\nu\omega,L}^- = I_{\nu\omega}^-(\xi = \xi_L, \vartheta, \varphi)$ are the forward and backward intensities at the interfaces, just inside the medium; $\xi = x/(1/k_\nu)$ is the spectral optical path, $1/k_\nu$ being the radiative extinction length; $\xi_L = L/(1/k_\nu)$ is the optical thickness, L being the slab thickness.

2.2. Radiative boundary conditions

Proper radiative boundary conditions will allow to determine the interface forward and backward intensities. For a transparent interface, see Fig. 5, the boundary condition has to take into account both the radiation transmitted trough the interface inside the medium and the radiation reflected internally from medium; in particular they can be written as:

$$I_{\nu\omega,0}^+ = \frac{1}{\pi}\int_0^{2\pi}\int_0^1 \mathbf{t}_{\nu,\omega^*\to\omega} I_{\nu\omega^*,0}^{+\mathrm{ext}}\mu^*\,\mathrm{d}\mu^*\,\mathrm{d}\phi^* + \frac{1}{\pi}\int_0^{2\pi}\int_0^1 \mathbf{r}_{\nu,\omega^*\to\omega} I_{\nu\omega^*,0}^-\mu^*\,\mathrm{d}\mu^*\,\mathrm{d}\phi^* \tag{4}$$

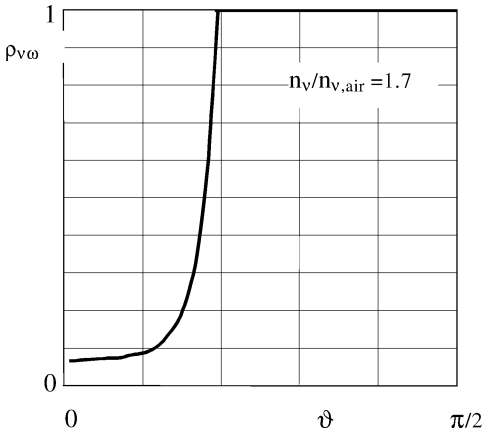

Fig. 5. Internal reflection.

$$I^{-}_{\nu\omega,L} = \frac{1}{\pi}\int_0^{2\pi}\int_0^{1} \mathbf{t}_{\nu,\omega^*\to\omega} I^{-\,\mathrm{ext}}_{\nu\omega^*,L}\mu^*\,\mathrm{d}\mu^*\,\mathrm{d}\phi^* + \frac{1}{\pi}\int_0^{2\pi}\int_0^{1} \mathbf{r}_{\nu,\omega^*\to\omega} I^{+}_{\nu\omega^*,L}\mu^*\,\mathrm{d}\mu^*\,\mathrm{d}\phi^* \tag{5}$$

where: $\mathbf{t}_{\nu\omega^*\to\omega}$ and $\mathbf{r}_{\nu\omega^*\to\omega}$ are the spectral bidirectional transmission and reflection distribution functions at interface; $I^{+\,\mathrm{ext}}_{\nu\omega^*,0}$ and $I^{-\,\mathrm{ext}}_{\nu\omega^*,L}$ are the external intensities incident on the two interfaces, see Fig. 4. The term $\mathbf{t}_{\nu\omega^*\to\omega}\mu^*\,\mathrm{d}\mu^*\,\mathrm{d}\phi^*/\pi$ represents the fraction of the radiation coming from the direction $\omega^*(\vartheta^*,\varphi^*)$ and contained within the angle $\mathrm{d}\omega^*$ which is transmitted in the direction $\omega(\vartheta,\varphi)$ and contained within the angle $\mathrm{d}\omega$.

The above expressions can be consistently simplified since for the processes and the wavelength of interest the surfaces of the slab are optically smooth. In this case the radiative interface phenomena are described by means of the Snell and Fresnel relations, in terms of the ratio of the complex refractive indices of the two media. For a slab embedded in air, the complex ratio simplifies in: $(n_\nu/n_{\nu,\mathrm{air}}) + i(n^*_\nu/n_{\nu,\mathrm{air}})$, where the imaginary part, n^*_ν, is related to the slab absorption coefficient, k_ν. For the usual values of the absorption coefficient of semitransparent plastics and for wavelengths typical of IR instruments, the interface relations are further simplified being: $n^*_\nu/n_{\nu,\mathrm{air}} \to 0$.

The energy interface phenomena can be expressed in terms of the spectral directional transmittivity ($\tau_{\nu\omega}$) or reflectivity ($\rho_{\nu\omega} = 1 - \tau_{\nu\omega}$), defined with reference to the radiative energy balance equation at interface; for example at $\xi = 0$, one has:

$$\left(I^{+\,\mathrm{ext}}_{\nu\omega,0} - I^{-\,\mathrm{ext}}_{\nu\omega,0}\right)\mu^*\,\mathrm{d}\omega^*\,\mathrm{d}\phi^*\,\mathrm{d}\nu = I^{+}_{\nu\omega,0}\mu\,\mathrm{d}\omega\,\mathrm{d}\phi\,\mathrm{d}\nu \tag{6}$$

$$\begin{aligned}\rho_{\nu\omega} &= I^{-\,\mathrm{ext}}_{\nu\omega,0}/I^{+\,\mathrm{ext}}_{\nu\omega,0}\\ \tau_{\nu\omega} &= \left(I^{+}_{\nu\omega,0}/I^{+\,\mathrm{ext}}_{\nu\omega,0}\right)(n_\nu/n_{\nu,\mathrm{air}})^2\\ 1-\rho_{\nu\omega} &= \tau_{\nu\omega}\end{aligned} \tag{7}$$

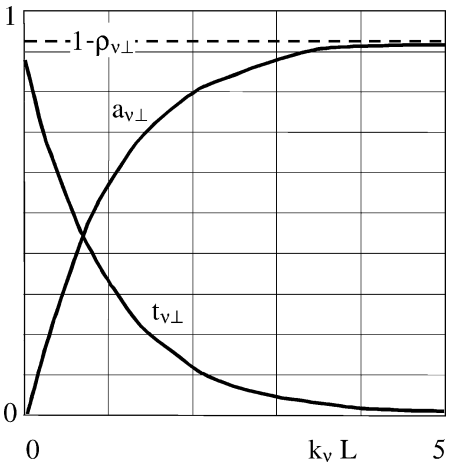

Fig. 6. Slab absorptance and transmittance.

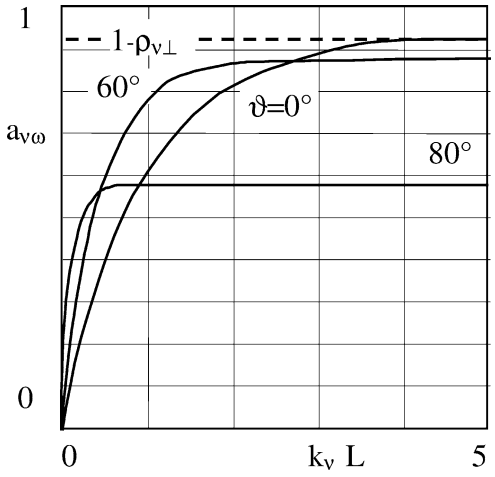

Fig. 7. Slab absorptance.

where: $\mathrm{d}\nu^* = \mathrm{d}\nu$; $\mathrm{d}\omega = \sin(\vartheta)\,\mathrm{d}\vartheta\,\mathrm{d}\phi = -\mathrm{d}\mu\,\mathrm{d}\phi$; $\mathrm{d}\omega^* = -\mathrm{d}\mu^*\,\mathrm{d}\phi^*$; the Snell law gives: $\mathrm{d}\phi^* = \mathrm{d}\phi$; $\mu^{*2} - 1 = (\mu^2 - 1)(n_\nu/n_{\nu,\mathrm{air}})^2$.

The above equation may be read considering the energy flux incident on the surface, $I^{+\,\mathrm{ext}}_{\nu\omega,0}\mu^*\,\mathrm{d}\omega^*\,\mathrm{d}\phi^*\,\mathrm{d}\nu$: a fraction is reflected, $I^{-\,\mathrm{ext}}_{\nu\omega,0}\mu^*\,\mathrm{d}\omega^*\,\mathrm{d}\phi^*\,\mathrm{d}\nu$, and a fraction is transmitted trough the surface, $I^{+}_{\nu\omega,0}\mu\,\mathrm{d}\omega\,\mathrm{d}\phi\,\mathrm{d}\nu$, and refracted in a new direction condensing in a new solid angle.

Strictly speaking the transmittivity and reflectivity depend on the state of polarization of radiation, but, considering a circularly polarized radiation, they can be assumed as the mean value of two components, see Figs. 6 and 7.

For an optically smooth surface, the bidirectional transmission and reflection distribution functions are related to the transmittivity and reflectivity as:

$$\mathbf{r}_{\nu,\omega^*\to\omega} = \left(\pi/\mu^*\right)\rho_{\nu\omega}\delta\left(\mu^* - \mu\right)\delta\left[\varphi^* - (\varphi + \pi)\right] \tag{8}$$

$$\begin{aligned}\mathbf{t}_{\nu,\omega^*\to\omega} = {}& \left(\pi/\mu^*\right)(n_\nu/n_{\nu,\mathrm{air}})^2\tau_{\nu\omega}\\ &\times \delta\left(\mu^* - \left[1 - \left(\mu^2 - 1\right)(n_\nu/n_{\nu,\mathrm{air}})^2\right]^{1/2}\right)\\ &\times \delta\left[\varphi^* - \left(\varphi^* + \pi\right)\right]\end{aligned} \tag{9}$$

$\delta(x - x_0)$ being the Dirac delta and the radiative boundary conditions simplify as:

$$I^{+}_{\nu\omega,0} = \tau_{\nu\omega}(n_\nu/n_{\nu,\mathrm{air}})^2 I^{+\mathrm{ext}}_{\nu\omega,0} + \rho_{\nu\omega} I^{-}_{\nu\omega,0} \tag{10}$$

$$I^{-}_{\nu\omega,L} = \tau_{\nu\omega}(n_\nu/n_{\nu,\mathrm{air}})^2 I^{-\mathrm{ext}}_{\nu\omega,L} + \rho_{\nu\omega} I^{+}_{\nu\omega,L} \tag{11}$$

2.3. The hot and cold slab

Once the radiative boundary conditions are known, the radiation field in the slab and in particular the radiation leaving the slab can be obtained.

The problem being linear, the radiative field can be sought as resulting from the sum of two simpler problems: the "hot slab", in which the radiation is only due to emission and the "cold slab", in which the radiation is only due to external forward and backward radiation.

2.3.1. The hot slab

In this case the radiative field is due only to the emission of radiation, thus Eqs. (2) and (3) still hold, but $I^{+\mathrm{ext}}_{\nu\omega^*,0} = I^{-\mathrm{ext}}_{\nu\omega^*,0} = 0$. It can be shown that the intensities at the interfaces are given by:

$$I^{+}_{\nu\omega,0} = \left[\rho_{\nu\omega}/\left(1 - \rho^2_{\nu\omega}T^2_{\nu\omega}\right)\right]\left(J^{+}_{\nu\omega} + \rho_{\nu\omega}T_{\nu\omega}J^{-}_{\nu\omega}\right) \tag{12}$$

$$I^{-}_{\nu\omega,L} = \left[\rho_{\nu\omega}/\left(1 - \rho^2_{\nu\omega}T^2_{\nu\omega}\right)\right]\left(\rho_{\nu\omega}T_{\nu\omega}J^{+}_{\nu\omega} + J^{-}_{\nu\omega}\right) \tag{13}$$

where $T_{\nu\omega} = \exp(-\xi_L/\mu)$ is the spectral directional beam transmittance, $J^{+}_{\nu\omega}$ and $J^{-}_{\nu\omega}$ are the auxiliary bulk functions defined such as:

$$J^{+}_{\nu\omega} = \int_0^{\xi_L} n^2_\nu I_{\mathrm{b}\nu}\left[T\left(\xi^*\right)\right] \mathrm{e}^{-\xi^*/\mu}\,\mathrm{d}(\xi^*/\mu)$$

$$J^{-}_{\nu\omega} = \int_0^{\xi_L} n^2_\nu I_{\mathrm{b}\nu}\left[T\left(\xi^*\right)\right] \mathrm{e}^{-(\xi_L-\xi^*)/\mu}\,\mathrm{d}(\xi^*/\mu)$$

Finally, the radiation leaving the hot slab is given by:

$$\begin{aligned} I^{+\mathrm{ext}}_{\nu\omega,L} &= (n_{\nu,\mathrm{air}}/n_\nu)^2 \tau_{\nu\omega} I^{+}_{\nu\omega,L} \\ &= (n_{\nu,\mathrm{air}}/n_\nu)^2 \tau_{\nu\omega}\left(I^{+}_{\nu\omega,0}T_{\nu\omega} + J^{-}_{\perp,\nu}\right) \end{aligned} \tag{14}$$

2.3.2. The cold slab

In this case, the radiative filed is due only to the external backward and forward radiation impinging on the slab, thus $I_{\mathrm{b}\nu}[T(\xi^*)] = 0$.

The radiative field is simplified because $J^{+}_{\nu\omega} = J^{-}_{\nu\omega} = 0$. Considering a slab subjected only to the external forward radiation one has:

$$\begin{aligned} I^{+}_{\nu\omega}(\xi) &= I^{+}_{\nu\omega,0}\exp(-\xi/\mu) \\ I^{-}_{\nu\omega}(\xi) &= I^{-}_{\nu\omega,L}\exp\left[-(\xi_L - \xi)/\mu\right] \end{aligned} \tag{15}$$

where: $I^{+}_{\nu\omega,0} = \rho_{\nu\omega}I^{-}_{\nu\omega,L}T_{\nu\omega} + \tau_{\perp\nu}(n_\nu/n_{\nu,\mathrm{air}})^2 I^{+\mathrm{ext}}_{\nu\omega,0}$ and $I^{-}_{\nu\omega,L} = \rho_{\nu\omega}I^{+}_{\perp\nu,0}T_{\nu\omega}$.

Once the radiative field is derived, the transmitted intensity leaving the slab and the backward reflected one can be expressed in terms of the spectral directional slab transmittance and reflectance, $t_{\nu\omega}$ and $r_{\nu\omega}$, defined as:

$$t_{\nu\omega} = I^{+\mathrm{ext}}_{\nu\omega,L}/I^{+\mathrm{ext}}_{\nu\omega,0} = (1-\rho_{\nu\omega})^2 T_{\nu\omega}/\left[1 - \rho^2_{\nu\omega}T^2_{\nu\omega}\right] \tag{16}$$

$$\begin{aligned} r_{\nu\omega} &= I^{-\mathrm{ext}}_{\nu\omega,0}/I^{+\mathrm{ext}}_{\nu\omega,0} \\ &= \rho_{\nu\omega} + \left[(1+\rho_{\nu\omega})^2\rho_{\nu\omega}T^2_{\nu\omega}\right]/\left[1 - \rho^2_{\nu\omega}T^2_{\nu\omega}\right] \end{aligned} \tag{17}$$

There are no further parameters to specify since the spectral directional slab absorptance is related to the transmittance and reflectance by an overall energy balance: $1 = r_{\nu\omega} + t_{\nu\omega} + a_{\nu\omega}$.

As an example, in Figs. 8 and 9, the spectral slab absorptance and transmittance are reported vs optical thickness, for $n_\nu/n_{\nu,\mathrm{air}} = 1.72$, typical value for plastic corresponding to $\rho_{\nu\perp} = 0.07$. The plots of Fig. 8 show that, for increasing value of the optical thickness, the absorptance increase, going to constant value, $a_{\nu\perp} = 1 - \rho_{\nu\perp}$, and the transmittance decrease, going to zero; for optical thin limit, $\xi_L \to 0$, the absorptance vanishes and the transmittance goes to: $t_{\nu\perp} = (1-\rho_{\nu\perp})/(1+\rho_{\nu\perp})$. The curves presented in Fig. 8 reveal that: for optical thick limit, $\xi_L \to \infty$, the radiative phenomenon turns out to be a surface one and the absorptance decreases as the incidence angle increases,

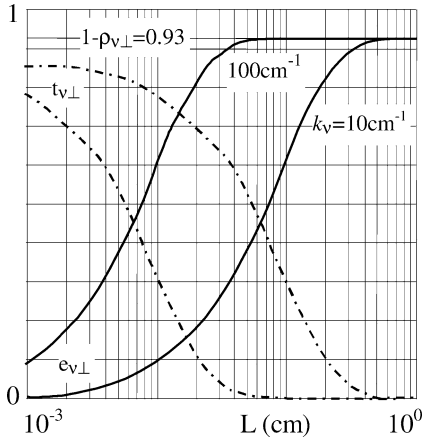

Fig. 8. Spectral normal slab emittance.

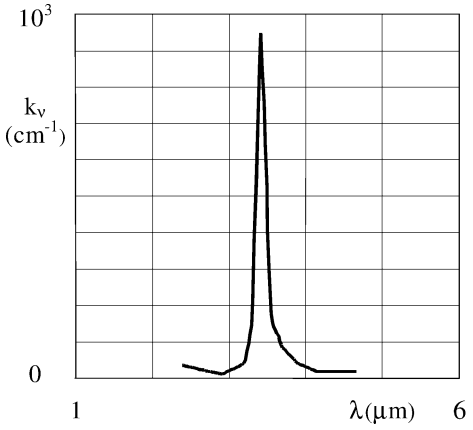

Fig. 9. Absorption spectrum for pp.

$a_{\nu\omega} = 1 - \rho_{\nu\omega}$; for optical thin limit, the behaviour is the opposite because the beam transmittance effect is greater than the reflection interface one.

3. The isothermal slab

Consider a slab at known uniform temperature, T_{slab}, immersed in air and confined by a surrounding with known radiation field, that is for specified $I^{+\text{ext}}_{\nu\omega,0}$ and $I^{-\text{ext}}_{\nu\omega,L}$. The radiative boundary conditions are:

$$I^{+}_{\nu\omega,0} = \rho_{\nu\omega} I^{-}_{\nu\omega,0} + \tau_{\nu\omega}(n_\nu/n_{\nu,\text{air}})^2 I^{+\text{ext}}_{\nu\omega,0} \tag{18}$$

$$I^{-}_{\nu\omega,L} = \rho_{\nu\omega} I^{+}_{\nu\omega,L} + \tau_{\nu\omega}(n_\nu/n_{\nu,\text{air}})^2 I^{-\text{ext}}_{\nu\omega,L} \tag{19}$$

In this case the hot slab solution simplifies because it will result: $J^{+}_{\nu\omega} = -J^{-}_{\nu\omega} = 1 - T_{\nu\omega}$ and the radiative field can be easily obtained in closed form.

The intensity leaving the slab due to emission can be obtained in terms of the spectral directional slab emittance, defined as:

$$\begin{aligned} \mathrm{e}_{\nu\omega} &= I^{+\text{ext}}_{\nu\omega,L} / \left(n^2_{\nu,\text{air}} I_{\text{b}\nu,\text{slab}}\right) \\ &= (1-\rho_{\nu\omega})[1-T_{\nu\omega}]/[1-\rho_{\nu\omega}T_{\nu\omega}] \end{aligned} \tag{20}$$

As expected, the spectral directional emittance is not revealed to be an extra radiative bulk parameter to specify, because it is equal to the spectral directional absorptance.

3.1. Basic spectral functions

As observed before, for the isothermal slab the spectral directional radiative response is completely described by two functions: slab emittance and transmittance, which turn out to depend on the spectral radiative parameters of the slab material and the slab thickness, that is: $n_\nu/n_{\nu,\text{air}}$, the spectral relative refractive index, and $\xi_L = k_\nu L$, the spectral optical thickness.

Fig. 10 shows the spectral normal slab emittance vs slab thickness for different absorption coefficients and $\rho_{\nu\perp} = 0.07$. For high values of the thickness measured with respect to the absorption length, $L/(1/k_\nu) \gg 1$, the emittance attains constant value, recovering the limit behaviour of optically thick slab, whereas while for $L/(1/k_\nu) \ll 1$, the optically thin approximation is recovered: the slab absorbs and emits little so the emittance tends to vanish. For increasing values of absorption coefficient, the curves are shifted on the left, the optical thick limit being recovered for lower values of thickness.

3.2. The semitransparent slab

In Fig. 11, the absorption spectrum for PP is reported. The shape is typical for most polymer characterised by the C–H bond: its main feature is the peak around 3.43 μm. To simplify the description which follows and to evidence the relevant aspect to which the semitransparent slab behaviour

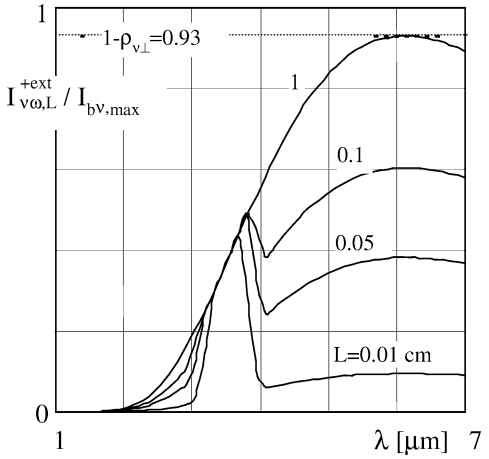

Fig. 10. Leaving intensity for $k_{\max}/k_{\min} = 100$.

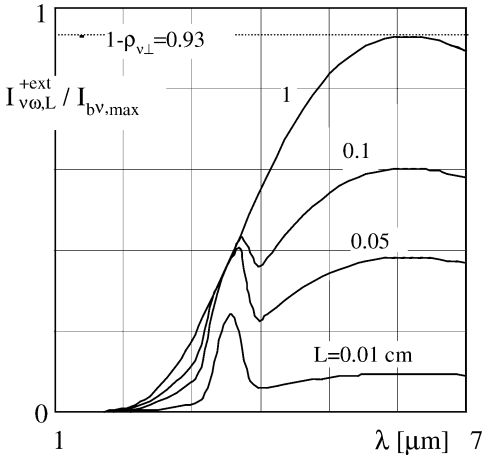

Fig. 11. Leaving intensity for $k_{\max}/k_{\min} = 10$.

is related, the absorption spectrum will be characterised with a single absorption band, described by a Gaussian curve, centred at λ_0 with wavelength amplitude $\Delta\lambda$, as:

$$(k_\nu/k_{\min})/(k_{\max}-k_{\min}) = \exp\left[-(\lambda-\lambda_0)^2/\Delta\lambda^2\right] \tag{21}$$

where: $k_{\min}$ is the absorption coefficient far from the absorption band and $k_{\max}$ is the maximum value attained inside the band. The following values are assumed: $k_{\min} = 10\ \text{cm}^{-1}$, $\lambda_0 = 3.5\ \mu\text{m}$, $\Delta\lambda = 0.2\ \mu\text{m}$. This choice makes it possible to consider a variable peak intensity: the absorption coefficient ratio, $k_{\max}/k_{\min}$, remains the only the free parameter to describe the radiative behaviour of the slab material. Concerning the polymer refraction index, its variation in the region around the peak results to be limited and so a constant value is assumed $n_\nu/n_{\nu,\text{air}} = 1.72$, which leads to $\rho_{\perp\nu} = 0.07$.

For the above assumptions the leaving intensity turns out to depend on the slab and ambient temperature, the absorption coefficient ratio $k_{\max}/k_{\min}$ and the slab thickness; this dependence is shown in Figs. 12 and 13, for different thickness and two slab materials, $k_{\max}/k_{\min} = 100$ and $k_{\max}/k_{\min} = 10$, respectively. For sake of simplicity, a slab at high temperature, such that $T_{\text{amb}}/T_{\text{slab}} \to 0$, is

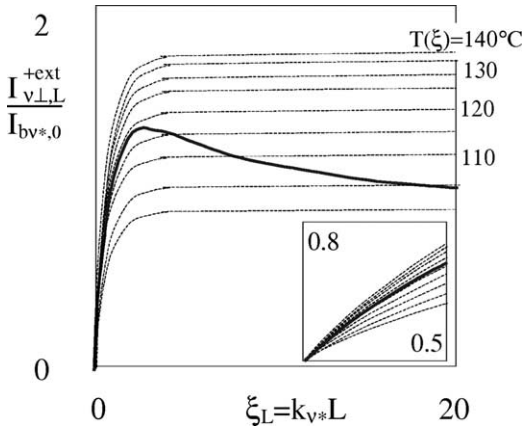

Fig. 12. Leaving intensity for non-isothermal slab.

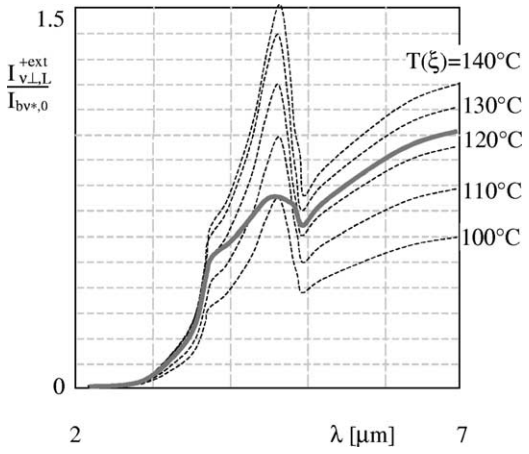

Fig. 13. Leaving intensity for non-isothermal slab.

considered, with $T_{\text{slab}} = 200\,^{\circ}\text{C}$; the spectral intensities are reported in dimensionless form with respect to the maximum spectral intensity of the blackbody at T_{slab}, $I_{b\nu,\max}$. The plots reveal that, at low thickness, the emitted intensity markedly resembles the fingertip of the spectral absorption coefficient; this effect tends to vanish for increasing thickness, that is approaching the opaque slab limit.

4. The non-isothermal slab

Once the temperature distribution across the slab is known, the spectral radiative field due to emission can be calculated, but not in the close form as for the isothermal slab. This limitation can be removed if the black body Plank function is approximated by a power series:

$$I_{b\nu}\big[T(\xi)\big] = I_{b\nu,0} + \sum_{n=1,\ldots,N} C_{\nu,n}\xi^n$$

$$I_{b\nu,0} = I_{b\nu}\big[T(\xi=0)\big]$$

in this case the radiative field due to emission can be obtained in closed form again, $J^+_{\nu\omega}$ and $J^-_{\nu\omega}$ being known:

$$J^+_{\nu\omega}/n^2_\nu = I_{b\nu,0}(1-T_{\nu\omega}) + \sum_{n=1,\ldots,N} C_{\nu,n}\mu^n F^+_{\nu\omega,n}$$

$$J^-_{\nu\omega}/n^2_\nu = I_{b\nu,0}(T_{\nu\omega}-1) + T_{\nu\omega}\sum_{n=1,\ldots,N} C_{\nu,n}\mu^n F^-_{\nu\omega,n}$$

where the auxiliary functions $F^+_{\nu\omega,n}$ and $F^-_{\nu\omega,n}$ are given by:

$$F^+_{\nu\omega,n} = \int_0^{\xi_L/\mu} y^n\,\mathrm{e}^{-y}\,\mathrm{d}y$$

$$F^+_{\nu\omega,n} = nF^+_{\nu\omega,n-1} - (\xi_L/\mu)^n T_{\nu\omega}$$

$$F^+_{\nu\omega,0} = 1/n$$

$$F^-_{\nu\omega,n} = \int_0^{\xi_L/\mu} y^n\,\mathrm{e}^{y}\,\mathrm{d}y$$

$$F^-_{\nu\omega,n} = -nF^-_{\nu\omega,n-1} + (\xi_L/\mu)^n/T_{\nu\omega}$$

$$F^-_{\nu\omega,0} = 1/n$$

$$J^+_{\nu\omega} = \int_0^{\xi_L} n^2_\nu I_{b\nu}\big[T(\xi^*)\big]\,\mathrm{e}^{-\xi^*/\mu}\,\mathrm{d}(\xi^*/\mu)$$

$$J^-_{\nu\omega} = \int_0^{\xi_L} n^2_\nu I_{b\nu}\big[T(\xi^*)\big]\,\mathrm{e}^{-(\xi_L-\xi^*)/\mu}\,\mathrm{d}(\xi^*/\mu)$$

In the following the technique is applied to a slab supposed to exhibit a parabolic temperature distribution: $(T(\xi)-T_0)/(T_{\max}-T_0) = \xi(\xi_L-\xi)$, with $T_0 = 100\,^{\circ}\text{C}$ and $T_{\max} = 140\,^{\circ}\text{C}$; the corresponding Plank function distribution across the slab results to be a know function, whose shape depends on the wavelength and on the ratio $I_{b\nu,\max}/I_{b\nu,0}$. In order to evidence the main feature of the non-isothermal slab, the shape is fixed choosing a reference wavelength as $\lambda_r = 5$ μm. Then, the Plank function can be approximated by a second order power series:

$$(I_{b\nu_r} - I_{b\nu_r,0})/(I_{b\nu_r,\max} - I_{b\nu_r,0}) = 4\big[(\xi/\xi_L) - (\xi/\xi_L)^2\big]$$

with $I_{b\nu_r,\max}/I_{b\nu_r,0} = 2$.

The radiative field can be easily calculated and so the radiation leaving the slab.

In Fig. 14, the radiation leaving the slab normalized with respect to the black body intensity evaluated at the wall temperature and $\lambda_r = 5$ μm, $I_{b\nu_r,0}$, vs the optical length is presented for a transparent grey slab. For reference the curves related to isothermal slabs are also reported. The radiation leaving the slab is the same as that from an isothermal slab whose temperature is contained within the minimum wall and maximum temperature. In the limit of thick slab the emission approaches to that of an isothermal slab mantained at wall temperature, i.e., the slab behaves as an opaque body; in the optical thin limit, the equivalent isothermal temperature is about 122 °C.

In Fig. 15, the radiation leaving the slab vs the wavelength is presented for given a semitransparent slab, $k_{\max}/k_{\min} =$

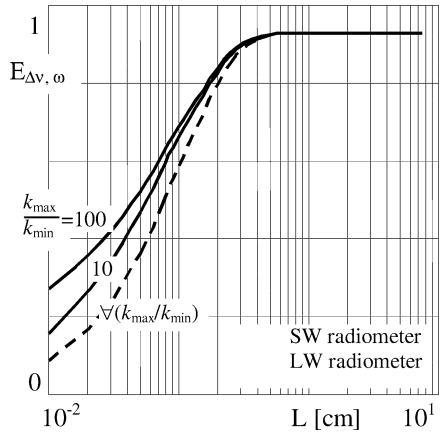

Fig. 14. Basic radiometer-slab function for $t = 200\,^{\circ}\mathrm{C}$ for different semitransparent slabs.

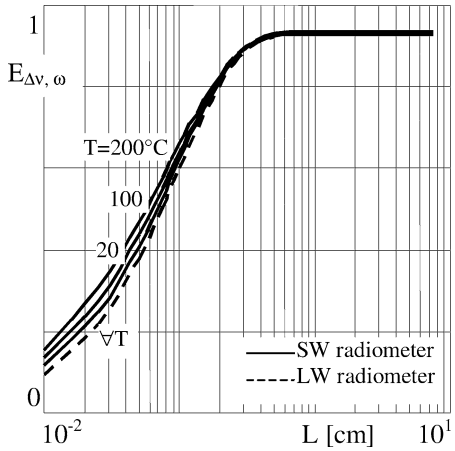

Fig. 15. Basic radiometer-slab function for a given semitransparent slab ($k_{max}/k_{min} = 100$).

100 and $L = 0.05$ cm. The spectrum shows that: for wavelengths far from the absorption coefficient peak, the slab behaves like optical thin slab and emits as an equivalent isothermal one at 122 °C; in the region around the peak, the curve approaches the one related to the wall temperature.

5. IR radiometer measurements

In the above paragraphs, explicit formulas have been presented to determine the radiative field in an slab with a given temperature profile across the thickness, once the radiative behaviour of slab and the external radiation impinging are known.

In the following, the precedent discussion, is focused on the fundamental IR radiometer problem with plastics, that is how to infer the temperature of an isothermal semitransparent slab and how to characterize the case of non-isothermal semitransparent slabs.

It will be assumed that the air attenuation along the path between the target and the radiometer can be neglected because of the low values of the optical path in the infrared region: the radiation shooting the radiometer is the same leaving the target. The radiation stimulates the detector according to the radiometer spectral transfer function, that is the spectral transmittance of the optical system and the spectral detector sensitivity. In the following, for convenience and without loss of generality, an ideal radiometer will be considered, i.e., one for which the transfer function assumes a constant value in the radiometer sensitivity band. The response of two different radiometers will be considered: a short wave, SW, infrared radiometer, with sensitivity band of $\Delta\lambda = 2$–5 μm; a long wave, LW, infrared radiometer, with sensitivity band of $\Delta\lambda = 8$–12 μm.

5.1. The isothermal semitransparent slab

For an isothermal slab embedded in air and confined by a surrounding at known temperature, T_{amb}, the slab radiosity measured by radiometer within its sensitivity band, $I_{\Delta\nu,\omega}$, is a combination of radiation emitted from, reflected from and transmitted through the slab:

$$I_{\Delta\nu,\omega} = \int_{\Delta\lambda} I^{+\,\mathrm{ext}}_{\nu\omega,L}\,\mathrm{d}\lambda = I_{\mathrm{b,slab}}\,e_{\Delta\nu,\omega} + I_{\mathrm{b,amb}}(1 - a_{\Delta\nu,\omega}) \tag{22}$$

$$e_{\Delta\nu,\omega} = \int_{\Delta\lambda} I_{\mathrm{b}\nu,\mathrm{slab}}\,e_{\nu\omega}\,\mathrm{d}\lambda / I_{\mathrm{b,slab}}$$
$$a_{\Delta\nu,\omega} = \int_{\Delta\lambda} I_{\mathrm{b}\nu,\mathrm{amb}}\,e_{\nu\omega}\,\mathrm{d}\lambda / I_{\mathrm{b,amb}} \tag{23}$$

where: $I_{\mathrm{b,slab}} = \int_{\Delta\lambda} I_{\mathrm{b}\nu,\mathrm{slab}}\,\mathrm{d}\lambda$ and $I_{\mathrm{b,amb}} = \int_{\Delta\lambda} I_{\mathrm{b}\nu,\mathrm{amb}}\,\mathrm{d}\lambda$ are the blackbody intensities evaluated at T_{slab} and T_{amb}, respectively; $e_{\Delta\nu,\omega}$ and $a_{\Delta\nu,\omega}$ are the *radiometer-slab* emittance and absorptance. Note that the names adopted for the last $e_{\Delta\nu,\omega}$ and $a_{\Delta\nu,\omega}$ stress that botrh the parameters are related not only to the material, but also to the radiometer features.

As expected, the radiometer-slab emittance turns out to be not equal to the radiometer-slab absorptance; these parameters, both related to the spectral slab emittance $e_{\nu\omega}$, depend on the slab and ambient temperature, respectively.

In the limiting case of grey transparent slab, i.e., $\rho_{\nu\omega}$ and k_ν not depending on wavelength, the radiometer-slab emittance and absorptance turn out to be the same of the corresponding spectral functions: $e_{\Delta\nu,\omega} = e_{\nu\omega}$ and $a_{\Delta\nu,\omega} = a_{\nu\omega} = e_{\nu\omega}$; as a result they are independent of temperature. The radiometer infers the slab temperature by assuming the target to be a grey opaque body, so a single object radiative parameter is needed: the radiometer emissivity, $\varepsilon = e_{\nu\omega}$, the reflectivity being its complement to unit. Thus, the radiometer-slab emittance can be used to set the radiometer emissivity and the on line temperature readout can be performed by radiometer built-in software. Note, however, the meaning of the term related to the ambient contribution: for an opaque body it accounts only for the reflected radiation, whereas for the transparent slab with

foreground temperature equal to background temperature, it accounts for both reflected and transmitted energy.

The situation is quite different when considering a semitransparent slab, because the radiometer-slab emittance and absorptance turn out to be different. To infer the slab temperature, the automatic emissivity correction mode cannot be used and a suitable software must to be used to accomplish the following tasks:

- read the target radiosity measured by the radiometer, $I_{\Delta\nu,\omega}$
- $I_{\mathrm{b,slab}}e_{\Delta\nu,\omega} + I_{\mathrm{b,amb}}(1 - a_{\Delta\nu,\omega})$
- calculate the radiometer slab absorptance, $a_{\Delta\nu,\omega}$, for a known ambient temperature, and subtract the ambient contribution to the target radiosity to obtain the emitted radiation
- solve for the slab temperature, since the emitted radiation calculated at the previous step, because of Eq. (24), is related to $I_{\mathrm{b,slab}}e_{\Delta\nu,\omega}$ both depending on the slab temperature.

In summary, in order to determine the slab temperature by radiometric measurements in semitransparent isothermal slabs, a single basic radiometer-slab function is needed:

$$E_{\Delta\nu,\omega} = \int_{\lambda_1}^{\lambda_2} I_{\mathrm{b}\nu}(T)e_{\nu\omega}\,\mathrm{d}\lambda \Big/ \int_{\lambda_1}^{\lambda_2} I_{\mathrm{b}\nu}(T)\,\mathrm{d}\lambda \tag{24}$$

this function will give the radiometer-slab emittance or absorptance depending on the selected temperature: $e_{\Delta\nu,\omega} = E_{\Delta\nu,\omega}(T_{\mathrm{slab}})$; $a_{\Delta\nu,\omega} = E_{\Delta\nu,\omega}(T_{\mathrm{amb}})$.

As an example, in Figs. 14 and 15, the radiometer-slab chart, that is a plot of the basic radiometer-slab function vs slab thickness, is drawn for different slab materials and temperatures. If the temperature is sought as the slab temperature, the radiometer-slab function meaning is related to the emitted radiation. The radiation detected by the radiometers increases with thickness, till to reach the opaque grey body limit. For the SW radiometer, the radiation increases as the absorption band peak increases, weakly depending on temperature. On the contrary the LW radiometer is not sensitive to presence of the absorption band, because it looks at the slab as a grey transparent body, and so the radiometer-slab emittance turns out to be independent of slab temperature. As expected, the SW radiometer receives an amount of radiative energy greater than the LW radiometer.

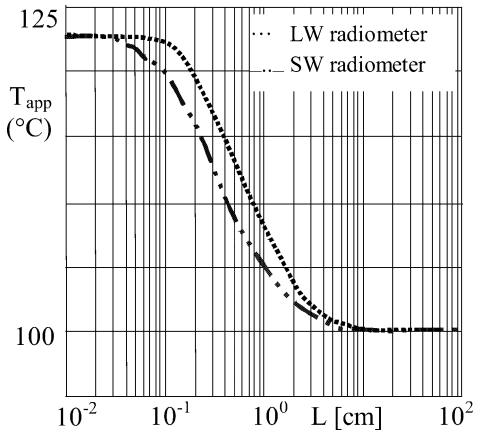

Fig. 16. Apparent temperature of semitransparent slab.

5.2. The non-isothermal semitransparent slab

A further problem arises when IR radiometer looks at a non-isothermal semi-transparent slabs with a temperature distribution across the thickness, $T = T(x)$.

The radiative field has been presented before: the intensity leaving the slab, $I_{\perp,\mathrm{IRR}}$, and measured by the radiometer results to be:

$$I_{\Delta\nu,\omega} = I^{e}_{\Delta\nu,\omega} + I_{\mathrm{b,amb}}(1 - a_{\Delta\nu,\omega}) \tag{25}$$

where $I^{e}_{\Delta\nu,\omega}$ is leaving intensity toward the slab, due to emission within the radiometer sensitivity band and, according to Eq. (15), is given by:

$$I^{e}_{\Delta\nu,\omega} = \int_{\lambda_1}^{\lambda_2} (n_{\nu,\mathrm{air}}/n_{\nu})^2 \tau_{\nu\omega}\left(I^{+}_{\nu\omega,0}T_{\nu\omega} + J^{-}_{\nu\omega}\right)\mathrm{d}\lambda \tag{26}$$

The radiation due to the ambient assumes the same form presented for the isothermal slab, because this contribution is not affected by slab temperature. This is not the case for the emitted radiation, related to the inner temperature distribution. In addition note that the spectral slab emittance looses its meaning: there is not a unique temperature related to the slab.

At this point, the procedure outlined for the isothermal case can be applied again with reference to the first two steps in order to calculate the emitted radiation. The third step seems to fail because the slab is not isothermal. To overcome this difficulty, the investigator must refer the known value of the emitted radiation to an equivalent problem characterised by a single temperature and strictly related to the problem under examination. It seems reasonable to refer to the same semitransparent slab, held at uniform temperature to emit the same radiation of the non-isothermal one. Therefore, the third step can still be applied so to obtain an apparent temperature, depending on the slab temperature distribution. The apparent temperature is expected to: coincide with the surface temperature for slab thickness increasing, i.e. approaching to the opaque body limit; attain an opportune average of the slab temperature distribution for thickness decreasing, that is approaching the optical thin slab limit.

As an example, in Fig. 16, the apparent temperature is reported versus slab thickness for $k_{\max}/k_{\min} = 100$, as seen by a SW and LW IR radiometers. Parabolic temperature distribution is assumed inside the slab, with surface temperature of 100 °C and maximum one of 140 °C.

For both radiometers, the apparent temperature recovers the surface one for optically thick slabs, whereas for decreasing thickness, it increases to reach a value of about 123 °C, very close to the average temperature across the slab. For a fixed thickness, the radiation sensed by LW radiometer comes more from the bulk rather than from the surface, and vice versa for the SW radiometer. Thus the apparent temperature readout results higher for LW than for SW radiometers. This suggests that two radiometers, sensitive in regions where the spectral absorption coefficients markedly differ, make it possible to have two distinct temperature values related to the slab temperature distribution; this happens if the slab radiative behaviour is far from the thin and thick limits.

Finally it has to be noted that, in the optical thin limit, the amount of radiation leaving the slab and hitting the radiometer attains is so slight that it is difficult to measure radiometrically.

6. Conclusions

Quantitative IR thermography can be applied to temperature measurement in the plastic film technology, but care must be taken when the materials and thickness are such that the film exhibit a semitransparent radiative behaviour. In this case the radiometer temperature readout cannot be performed by automatic emissivity correction mode, but by using offline a suitable software. The program is mainly based on the knowledge of the slab radiative field. The output from this field will give a reference temperature, that coincides with the slab temperature for an isothermal slab, whereas it is an apparent temperature for a non-isothermal slab. The apparent temperature is a sort of average value between the surface and bulk temperatures, shifted toward the surface value as the slab behaviour tends to the opaque limit. Radiometers sensible in different spectral regions will give different temperature readouts.

With reference to a non-isothermal transparent slab, the use of the radiometer seems to be limited, giving a single temperature. Further information can be obtained both working with different sensitivity bands, e.g., with different radiometers or adopting spectral filters, and looking at the target from different directions.

In facts the last procedure, does not provide additional information: as shwn by the above plots on the interface reflectivity of plastics, the internal cut-off angle results to be about 35 degrees and two region can be distinguished. In the first region the reflectivity assumes a constant value close to the one related to the normal direction: the leaving radiation is mainly affected by the value of the beam length, which in turn does not vary appreciably with respect to the normal one. In the second region the reflectivity exhibits a strong variation: the surface effect predominates, but the amount of energy leaving the slab is vanishing.

References

[1] J.F. Agassant, P. Avenas, J. Sergent, P.J. Carreau, Polymer Processing, Hanser, Munich, 1991.
[2] C. Rauwendaal, Polymer Extrusion, Hanser, Munich, 1986.
[3] P. Barq, J.M. Haudin, J.F. Agassant, Isothermal and anisothermal models for cast film extrusion, Internat. J. Polymer Processing 14 (1992) 334–349.
[4] S. D'Halewyu, J.F. Agassant, Y. Demay, Numerical simulation of the cast film process, Polymer Engrg. Sci. 30 (1990) 335–342.
[5] J.L. White, M. Cakmak, Adv. Polymer Technology 8 (1988) 27–61.
[6] D. Acierno, L. Di Maio, G. Cuccurullo, Analysis of temperature fields in film casting, Internat. J. Polymer Processing 19 (1999) 75–94.
[7] N. Hajji, J.E. Spruiell, Radiation pyrometry on semitransparent sheets I: Gray media, Polymer Engrg. Sci. 34 (1994).
[8] N. Hajji, J.E. Spruiell, Radiation pyrometry on semitransparent sheets II: Media with wavelength dependent absorption coefficient, Polymer Engrg. Sci. 34 (1994).
[9] W. Obendrauf, G.R. Langeker, W. Friesenbichler, Temperature measuring in plastics processing with infrared radiation thermometers, Internat. J. Polymer Processing 13 (1998).
[10] G. Cuccurullo, L. Di Maio, Velocity and thermal field thermography for thermoplastic polymers extrusion, in: Proceedings of Quantitative Infrared Thermography '96, 1996, pp. 287–292.
[11] P.G. Berardi, G. Cuccurullo, L. Di Maio, Thermography for polymers film blowing, in: Proceedings of Quantitative Infrared Thermography '98, 1998, pp. 265–271.
[12] C. Ammirati, L. Di Maio, G. Cuccurullo, D. Acierno, Heat exchange in film casting: modelling and experimental determination, in: Proceedings of Polymer Processing Society, 1996, pp. 313–314.
[13] P.G. Berardi, G. Cuccurullo, Radiation field in semi-transparent films for radiometric temperature measurement, in: Proceedings of 17th UIT National Heat Transfer Conference, 1999, pp. 493–502.
[14] G. Cuccurullo, P.G. Berardi, Radiometry of polymer film, Non destructive testing handbook infrared and thermal testing 3, in: ASNT, 2001, pp. 591–600.
[15] D.P. Dewitt, G.D. Nutter, Theory & Practice of Radiation Thermometry, Wiley, New York, 1989.
[16] R. Viskanta, E.E. Anderson, Heat transfer in semitransparent solids, Adv. Heat Transfer 11 (1975) 317–387.